OXFORD

Cerebral Cortex, 2025, **35**, bhaf043
https://doi.org/10.1093/cercor/bhaf043
Advance access publication date 18 March 2025
Original Article

A role for the insula in establishing social dominance: structural and functional MRI studies in nonhuman primates

Paul W. Czoty[1,†,*], Mohammad Kawas[2,3,†], Kedar Madi[2], Richard Barcus[2], Jeongchul Kim[2], Jeremy P. Hudson[2], Lindsey K. Galbo-Thomma[1], Hongyu Yuan[2], James B. Daunais[4], and Christopher T. Whitlow[2]

[1]Department of Translational Neuroscience, Wake Forest University School of Medicine, Medical Center Boulevard, Winston-Salem, NC 27157-1083, United States
[2]Department of Radiology, Wake Forest University School of Medicine, Medical Center Boulevard, Winston-Salem, NC 27157-1083, United States
[3]Department of Physiology & Biochemistry, School of Medicine, The University of Jordan, Amman, Jordan
[4]Department of Internal Medicine, Wake Forest University School of Medicine, Medical Center Boulevard, Winston-Salem, NC 27157-1083, United States
*Corresponding author: Paul W. Czoty, Department of Translational Neuroscience, Wake Forest University School of Medicine, Medical Center Boulevard, Winston-Salem, NC 27157-1083, United States. Email: pczoty@wakehealth.edu
[†]Paul W. Czoty and Mohammad Kawas contributed equally to this work.

Awareness of one's position in the social hierarchy is essential for survival. Conversely, poor social cognition is associated with several neuropsychiatric diseases. Although brain regions that mediate understanding of the social hierarchy are poorly understood, recent evidence implicates the insula. Magnetic resonance imaging (MRI) scans were acquired in twelve individually housed male cynomolgus monkeys to determine whether structural and functional characteristics of the insular cortex predicted the social rank that monkeys would attain once they formed stable social hierarchies. Structural MRI revealed that left insular volume was significantly larger in monkeys that would become dominant vs. subordinate. No differences were observed in other areas including amygdala, caudate nucleus, or prefrontal cortex. Volumetric differences were localized to dorsal anterior regions of both left and right insulae. Functional MRI revealed that global correlation, a measure of connectedness to the rest of the brain, was significantly lower in the left insula of monkeys who would become dominant vs. subordinate. Moreover, the fractional amplitude of low-frequency fluctuations, a reflection of spontaneous brain activity, trended lower in bilateral insula in the future dominant monkeys. This prospective study provides evidence for a role of the insula in the establishment and maintenance of social dominance relationships.

Keywords: MRI; nonhuman primates; social cognition; social dominance; subordination.

Introduction

The ability to accurately perceive one's social status relative to others is critical for successful social interactions. Impairments in identifying one's place in the social dominance hierarchy can be maladaptive in nonhuman primates (NHPs; Bernstein 1981; Sapolsky 2005), and poor social cognition has been identified as a source of vulnerability for development of several neuropsychiatric disorders in humans (eg Johnson et al. 2012). Studies of brain structure using magnetic resonance imaging (MRI) in humans demonstrated that social status and/or the perception of social dominance is related to gray matter volumes in several brain areas including the amygdala, prefrontal cortex and caudate nucleus (Chiao et al. 2009; Sallet et al. 2011; Noonan et al. 2014; Santamaria-Garcia et al. 2015; Watanabe and Yamamoto 2015). To extend neuroanatomical information, studies in humans have used functional MRI (fMRI) to identify brain areas that are active during the processing of social dominance information. These studies are consistently congruent with previous work in implicating the prefrontal cortex, amygdala and ventral striatum in the representation of social dominance (Zink et al. 2008, Chiao et al. 2009; Marsh et al. 2009; Farrow et al. 2011; Ly et al. 2011; Kumaran et al. 2012; Ligneul et al. 2016, 2017).

One limitation of studies of the neural basis of social dominance in humans is the reliance on cross-sectional designs and artificial laboratory scenarios. For example, it is not possible to determine whether differences in structure or function preceded or resulted from attainment of dominance status. Studies using NHPs, who naturally form linear social dominance hierarchies based on the outcomes of numerous social interactions, have helped to fill this gap (eg Sapolsky 2005; Kaplan et al. 2009). Decades of research in captive group-housed monkeys support the view that chronic social subordination is associated with physiological and neurobiological changes indicative of chronic stress. Although this relationship can differ in the wild and according to housing parameters (eg Abbott et al. 2003; Gesquiere et al. 2011), several lines of evidence support the view that, when housed in single-sex groups of four, subordinate monkeys experience chronic daily social stress (eg Czoty et al. 2009; Nader et al. 2012a, b). Moreover, dominant and subordinate monkeys can react differently to the same socially relevant stimuli

Received: September 9, 2024. **Revised:** January 9, 2025. **Accepted:** January 30, 2025

(eg Czoty and Nader 2012; Gould et al. 2017; Galbo-Thomma et al. 2023). To date, brain imaging studies in monkeys have largely agreed with human data in implicating the prefrontal cortex, amygdala and ventral striatum in the representation of social dominance (eg Sallet et al. 2011; Noonan et al. 2014; Munuera et al. 2018).

A growing body of evidence also implicates the insula in detection and processing of social dominance (eg Zink et al. 2008; Chiao et al. 2009; Santamaria-Garcia et al. 2015; Li et al. 2021) and higher-order socially relevant cognitive functions such as fairness, empathy and other aspects of social cognition (eg Hsu et al. 2008; Hu et al. 2016). The insula is a primary hub in the salience network, a group of brain regions that activate together in conditions that require integration of autonomic responses, emotions and internal goals with environmental stimuli (Downar et al. 2000; Seeley 2019). The anterior insula in NHPs is anatomically and functionally distinct from the posterior region (Jezzini et al. 2012; Evrard et al. 2014; Evrard 2019; Sypre et al. 2023). Anatomical, brain imaging, experimental and clinical literature support a similar anterior–posterior distinction in the human insula (eg Naqvi et al. 2007; Kurth et al. 2010; Cauda et al. 2012; Cerliani et al. 2012; Cloutman 2012; Chang et al. 2013; Uddin et al. 2017). Prevailing evidence suggests that the (dorsal) anterior portion primarily subserves its socio-affective and other socially relevant functions (eg Chiao et al. 2009; Zaki et al. 2012; Knobloch et al. 2024; Kim et al. 2023).

In the present study, MRI data were used to examine the structure and function of the insula in adult male cynomolgus monkeys prior to formation of social hierarchies to extend our understanding of the involvement of the insula in processing social status-related information. Monkeys were scanned when individually housed before being placed into social groups of four monkeys per pen. We examined whether measures of insular structure and function predicted the social rank monkeys would attain. Using structural MRI, insular volumes and shapes of future dominant and future subordinate monkeys were compared. Shape analysis provides a more granular view of morphological differences, highlighting regions of a structure where differences are greatest and providing a stronger link to understanding differences in insular function than gross volume comparisons alone. For example, shape analysis of the hippocampus has illuminated the relationship between brain aging and cognition, contributing to more efficient diagnosis of Alzheimer's disease (Voineskos et al. 2015; Katabathula et al. 2021). fMRI was used to examine the connectivity of the insula with other regions by determining global correlation (GCOR) maps, which characterize brain-wide connectedness, and maps of fractional amplitude of low-frequency fluctuations (fALFF) to compare and estimate differences in spontaneous brain activity in the insula providing complementary information about the degree of neuronal activity which is not captured by connectivity measures.

Materials and methods

Subjects

Twelve adult male cynomolgus monkeys (*Macaca fascicularis*) served as subjects. At the outset of the study, monkeys were housed individually in quadrants of stainless-steel cages (Allentown Caging, Allentown, New Jersey) in which water was available ad libitum. Monkeys were weighed weekly and fed enough food (Purina LabDiet Chow, St. Louis, MO), fresh fruit and vegetables daily to maintain healthy body weights without becoming obese as determined by daily inspection and periodic veterinary examinations. Body weights did not change significantly during these studies. Animal housing, handling, provision of environmental enrichment and all experimental procedures were performed in accordance with the *Guide for the Care and Use of Laboratory Animals* and were approved by the Animal Care and Use Committee of Wake Forest University (protocol #A21-030).

Social housing procedures and social rank determination

On average (± SD), monkeys were individually housed for 503 ± 20 days prior to being introduced to social groups. Details regarding the initiation of social housing and determination of social ranks for this cohort have been published previously (Galbo et al. 2022). Briefly, monkeys were initially singly housed in four quadrants of three pens separated by removable partitions, but with visual, auditory and limited tactile contact with each future pen-mate, for several weeks. During this time, MRI scans were completed as described below. On the first day of social housing, monkeys were introduced by removing the partitions in the cage. Partitions were replaced at ∼5:00 pm to prevent injury occurring when laboratory personnel were not present. After 1 week, they remained in social groups for 24 h each day. Over the next 12 weeks, social ranks were determined based on outcomes of agonistic encounters (see Galbo et al. 2022). Twice each week, each pen was video-recorded for 15 min while no personnel were present. Later, two observers viewed the videos and counted the number of several aggressive and submissive behaviors; both the initiator and recipient were recorded. The monkey in each pen aggressing towards and rarely submitting to all others was ranked #1 (most dominant). The monkey who aggressed towards all but the #1-ranked monkey and submitted only to him was designated #2-ranked, and so on. The #4-ranked monkey displayed the lowest frequency of aggressive behaviors and submitted to all other monkeys in the pen. Monkeys ranked #1- and #2-ranked were considered dominant and #3- and #4-ranked monkeys were considered subordinate.

MRI methods

Monkeys were 10.6 (±1.2) years old at the time of the MRI scan. Monkeys were initially anesthetized with 10 mg/kg ketamine and transported to the Wake Forest Translational Imaging Shared Resource where they were intubated. Anesthesia was maintained during the scan by 1.5% isoflurane; ketamine had worn off prior to data acquisition. Monkeys were artificially ventilated to maintain normal physiological parameters across animals and scan sessions. MRI data were acquired on a 3.0-Tesla Siemens Skyra scanner with a 32-channel pediatric head coil (Siemens AG, Erlangen, Germany). High-resolution 3-dimensional T1-weighted images were obtained using a magnetization-prepared rapid gradient echo sequence (MPRAGE): repetition time (TR) = 2700 ms; inversion time (TI) = 880 ms, echo time (TE) = 3.39 ms, slice thickness = 0.5 mm no gap; and in-plane resolution = 0.5 × 0.5 mm. For the resting-state blood oxygen level dependent (BOLD) MRI, a multi-band echo-planar imaging sequence was used with the following parameters: acceleration factor = 4, volumes = 848, repetition time (TR) = 700 ms, echo time = 32 ms, flip angle = 52°, number of slices = 32; slice thickness = 2 mm with 2 mm spacing, in-plane resolution = 2 × 2 mm and matrix = 64 × 64.

Structural MRI analysis

For volumetric analysis, the NHP-BrainExtraction tool was used (Wang et al. 2021) to skull-strip T1-weighted images. Then,

MR field inhomogeneity was corrected using the `N4BiasFieldCorrection` command of the Advanced Normalization Tools (ANTs; Penn Image Computing And Science Laboratory, University of Pennsylvania; Philadelphia, PA; Tustison et al. 2010). Next, the skull-stripped images were used to create a brain-only study specific template (SST), tissue probability maps and brain parcellation maps defined by the University of North Carolina NHP atlas. These were then warped to the SST using the *antsRegistrationSyN.sh* and `antsApplyTransforms` commands of ANTs. Next, the template-space probability and parcellation maps were warped to native space for each monkey using the transforms generated from the template creation process. These were then used to produce brain segmentations using the `antsAtroposN4` command of ANTs. Insular cortex volumes were then collected using FSL's `fslstats` tool (Jenkinson et al. 2012) and normalized to whole brain volume to adjust for differences in head size. Unpaired t-tests were performed to compare volumes of the right and left insulae of monkeys that became dominant versus subordinate.

Insula shape analysis

Insular segmentations were extracted from each monkey's parcellation maps as independent volumes, then registered to the insula of the UNC NHP atlas via FMRIB's Linear Registration Tool (FLIRT; Jenkinson and Smith 2001; Jenkinson et al. 2002). These volumes were then processed through the Spherical Harmonics Point Distribution Models (SPHARM-PDM) pipeline via SlicerSALT (Vicory et al. 2018), a shape analysis platform designed as a heavily customized version of the medical image analysis software, 3D Slicer (www.slicer.org). The SPHARM-PDM process (Styner et al. 2007) generates surface meshes that are used for subsequent shape analysis by converting binary segmentations of anatomical regions of interest into corresponding SPHARM descriptions; these are then sampled into PDMs ie triangulated surface meshes. Thus, each subject's input volume is standardized to a shape with a predetermined number of vertices (1,002 by default) to establish correspondence and ensure a valid quantitative comparison between all shapes, irrespective of each model's size or appearance.

The core premise of the SPHARM-PDM methodology is the processing and conversion of binary segmentations into surface meshes, which are then parameterized onto a unit sphere using an area-preserving, distortion-minimizing procedure (Brechbühler et al. 1995; Styner et al. 2006; Paniagua et al. 2013; Vicory et al. 2018). Every point i on the surface is assigned a parameter vector (φ_i, θ_i) and is mapped to exactly one point on the sphere, in accordance with their parameter vector. An initial parameterization is created using discrete Laplacian equations, and a constrained optimization procedure then ensures that (i) every object (ie surface) region is mapped to a region of proportional area in parameter space (area preservation), and (ii) every quadrilateral is mapped to a spherical quadrilateral in parameter space (minimal distortion) (Madi 2021). This procedure produces spherical harmonic coefficients that are the result of the mathematical equations described by Brechbühler (Brechbühler et al. 1995). Icosahedron subdivision of the spherical parameterization allows the uniform sampling and reconstruction of the final shape as a triangulated surface mesh as enabled by the spherical harmonic coefficients and the pre-computed parameter locations (φ_i, θ_i). Correspondence across all shape surfaces is established by aligning the spherical parameterizations of all shape models, using each shape's first order ellipsoid obtained from their respective spherical harmonic coefficients.

Once correspondence and alignment were established for all insular shape models, a statistical analysis was performed to visually identify surface regions of significant difference between future dominant and future subordinate monkeys using the Covariate Significance Testing module in SlicerSALT (Vicory et al. 2018). The module provides an interface for the Multivariate Functional Shape Data Analysis (MFSDA) method, a Python-based multivariate varying coefficient model that can efficiently correlate shape data with clinical and demographic variables such as age, gender, etc. The module functions to determine where any statistically significant morphological differences are present on a given shape and investigate what clinical variables and covariates are significantly associated with shape information in a given population. The MFSDA equation is defined as:

$$y_{ij}(d) = X_i^T \left[B_j(d) + n_{ij}(d) + e_{ij}(d) \right]$$

Variables and coefficients used in the above MFSDA equation are described in Michoud et al. (2019). Alignment and correspondence, as established during the SPHARM-PDM computation, are necessary to establish the association between correspondent surface nodes (ie vertices, in Cartesian coordinates) and the variables of interest. A color-coded "heat map" of p-values, corrected via false discovery rate, is overlaid upon the shape model of the atlas-generated insula; this map displays surface regions of significant difference in insular morphology between future dominant and future subordinate monkeys. To determine the directionality of the shape differences, mean insular shape models were generated for both groups using the principal component analysis module within SlicerSALT; both mean models were constructed by averaging the Cartesian coordinates along each correspondent vertex for all models in a group. Next, Euclidean distances were computed between correspondent vertices of the mean dominant insula and the mean subordinate insula via SlicerSALT's "Model To Model Distance" module, resulting in vectorized distances (in Cartesian notation) between the mean shape models. This process was performed for both the left and right insula. Visualization of statistical results and vector data was performed using the ParaView software (Ahrens et al. 2005).

fMRI processing

Processing and analysis pipelines were performed with the Statistical Parametric Mapping 12 (SPM12) software (http://www.fil.ion.ucl.ac.uk/spm/) and the CONN toolbox (release 20.b; Whitfield-Gabrieli and Nieto-Castanon 2012) running in MATLAB R2015b (MathWorks Inc., Natick, MA). Functional and anatomical data were preprocessed using a flexible preprocessing pipeline (Nieto-Castanon 2020a) including realignment, outlier detection, direct co-registration to structural data, direct segmentation, template-space normalization and smoothing. Functional data were co-registered to a reference image (the first volume of the scan session) using a least-squares approach and a six-parameter (rigid body) transformation (Friston et al. 1995), then resampled using b-spline interpolation. Potential outlier scans were identified using the Artifact Detection Tools software package (Whitfield et al. 2011) as acquisitions with framewise displacement above 0.9 mm or global BOLD signal changes above five standard deviations (Power et al. 2014; Nieto-Castanon 2022). Functional and anatomical data were co-registered using SPM's intermodality co-registration procedure (Ashburner and Friston 1997) with a normalized mutual information objective function (Studholme et al. 1998). Functional and anatomical data were

segmented into gray matter, white matter and cerebrospinal fluid (CSF) tissue classes, and resampled to 2-mm isotropic voxels following a direct normalization procedure (Calhoun et al. 2017; Nieto-Castanon 2022) using SPM's unified segmentation and normalization algorithm (Ashburner and Friston 2005; Ashburner 2007) with the SST tissue probability map. Functional data were smoothed using spatial convolution with a Gaussian kernel of 4-mm full-width half-maximum (FWHM). Post-processing visual quality checks were performed and led to the exclusion of two NHPs (one future dominant and one future subordinate) from fMRI analyses due to significant artifacts. In addition, functional data were denoised using a standard denoising pipeline (Nieto-Castanon 2020b), including the regression of potential confounding effects characterized by white matter timeseries (3 CompCor noise components), CSF timeseries (3 CompCor noise components), motion parameters (six factors; Friston et al. 1996), outlier scans (Power et al. 2014), and linear trends (two factors) within each functional run, followed by bandpass frequency filtering of the BOLD timeseries (Hallquist et al. 2013) between 0.01 Hz and 0.1 Hz. CompCor (Behzadi et al. 2007; Chai et al. 2012) noise components within white matter and CSF were estimated by computing the average BOLD signal as well as the largest principal components orthogonal to the BOLD average, motion parameters and outlier scans within each monkey's eroded segmentation masks.

fMRI-derived metrics and analysis

GCOR maps characterizing network centrality at each voxel were estimated as the average of all short- and long-range connections between a voxel and the rest of the brain (Saad et al. 2013). Connections were computed from the matrix of bivariate correlation coefficients between the BOLD timeseries from each pair of voxels, estimated using a singular value decomposition of the z-score normalized BOLD signal (subject-level SVD) with 64 components separately for each subject and condition (Whitfield–Gabrieli and Nieto-Castanon 2012). GCOR measures across voxels were rank-sorted and normalized separately for each subject using a Gaussian inverse cumulative distribution function with zero mean and unit variance. fALFF maps characterizing low-frequency BOLD signal variability at each voxel were estimated as the ratio between the root-mean-square of the BOLD signal after denoising and band-pass filtering between 0.01 Hz and 0.1 Hz, divided by the same measure computed before band-pass filtering (Zou et al. 2008). fALFF measures across voxels were then rank-sorted and normalized separately for each subject using a Gaussian inverse cumulative distribution function with zero mean and unit variance. GCOR and fALFF for the right and left insula were then generated by averaging these measures from all the voxels that comprise the insulae. These values were then used to perform independent t-tests to compare the values from future dominant and future subordinate monkeys.

Results

Social rank determination

The total number of aggressive and submissive behaviors observed in the three pens has been reported previously (Galbo et al. 2022).

Insular volume and shape differences

Monkeys that would eventually become dominant had significantly larger left insular volumes than those that would become subordinate ($t_{10} = 2.50$, $P = 0.031$). There was a trend of higher right insular volumes in future dominant monkeys ($t_{10} = 1.64$, $P = 0.131$; Fig. 1).

Analysis of insula shape indicated a greater density of significantly different surface regions on the left versus right insula. On the left insula (Fig. 2C), surface regions of highly significant difference included the anterior (granular) area of the dorsal fundus (Idfa), the dorsal dysgranular area (Idd), the mound dysgranular area (Idm) and the ventral dysgranular area (Idv). On the right insula (Fig. 2D), surface regions of significant difference included small portions of the Idd and Idm. Comparison of the mean left insula of future subordinates to the mean left insula of future dominant monkeys at these significantly different subregions (Fig. 2E) generated the following observations: (i) a slight posteroinferior depression (ie concavity) in the Idfa subregion, (ii) a posterolateral convexity (with slight bias towards the inferior) in the Idd subregion of the future dominant monkeys' insula, (iii) a posterolateral convexity in the Idm subregion of the future dominant monkeys' insula, and (iv) a small posteromedial depression in the Idv subregion of the future dominant monkeys' insula. Comparison of the mean right insula of future subordinates to the mean right insula of future dominant monkeys at these significantly different subregions (Fig. 2F) generated the following observations: (i) a posterolateral convexity that is more prevalent in the Idd subregion of the future dominant monkeys' insula, and (ii) a medial depression in the Idm subregion of the future dominant monkeys' insula.

Insular GCOR and fALFF analysis

Global correlation (a measure of global connectedness) across the left insula was significantly lower in future dominant monkeys ($t_8 = -2.86$, $P = 0.021$). There were no differences for the right insula ($t_8 = -0.19$, $P = 0.85$; Fig. 3). fALFF measures across the left and right insula trended lower in the future dominant monkeys ($t_8 = -1.97$, $P = 0.084$ and $t_8 = -2.07$, $P = 0.072$, respectively; Fig. 4).

Discussion

The primary aim of the present study was to prospectively examine whether the structure and/or connectivity of the insular cortex predicted the social rank that monkeys would attain once they were group-housed. MRI scans were conducted when monkeys were housed individually. Next, monkeys were placed into groups of four and dominance hierarchies developed that were linear and transitive (Galbo et al. 2022). Importantly, monkeys whose left insula was larger were more likely to assume a higher (dominant) rank; there was a trend for the right insula to be larger as well. Shape analysis determined that differences between future dominant and future subordinate monkeys were primarily in the anterior dorsal region of the insulae. The involvement of the anterior versus posterior insula is consistent with prior studies ascribing socio-affective function to this portion of the insula (eg Chiao et al. 2009; Zaki et al. 2012; Knobloch et al. 2024; Kim et al. 2023). For example, in an fMRI study in humans, subjects performed a cognitive task while competing against fictitious opponents identified as superior or inferior to the subject (Santamaria-Garcia et al. 2015). Electroencephalography was used to measure event-related potentials (ERP), representative of the brain's response to viewing opponents. Significant positive correlations were observed between the amplitude of the N170 component of the ERP signal (known to reflect face perception; Eimer 2011) and the social rank of the fictitious opponent. The magnitude of this effect correlated with cortical thickness of the insula and other brain regions.

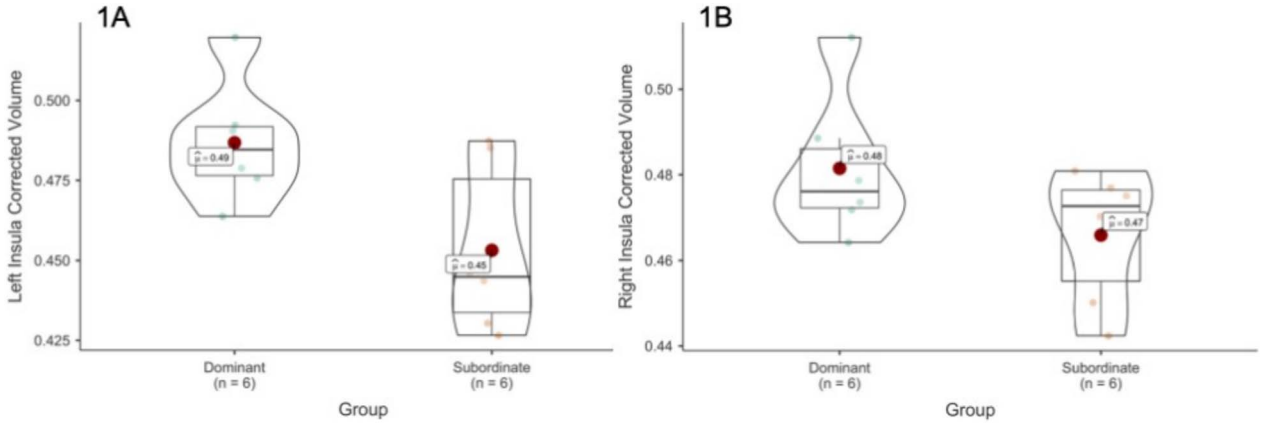

Fig. 1. Left (1A) and right (1B) insular volumes, corrected for total brain volume.

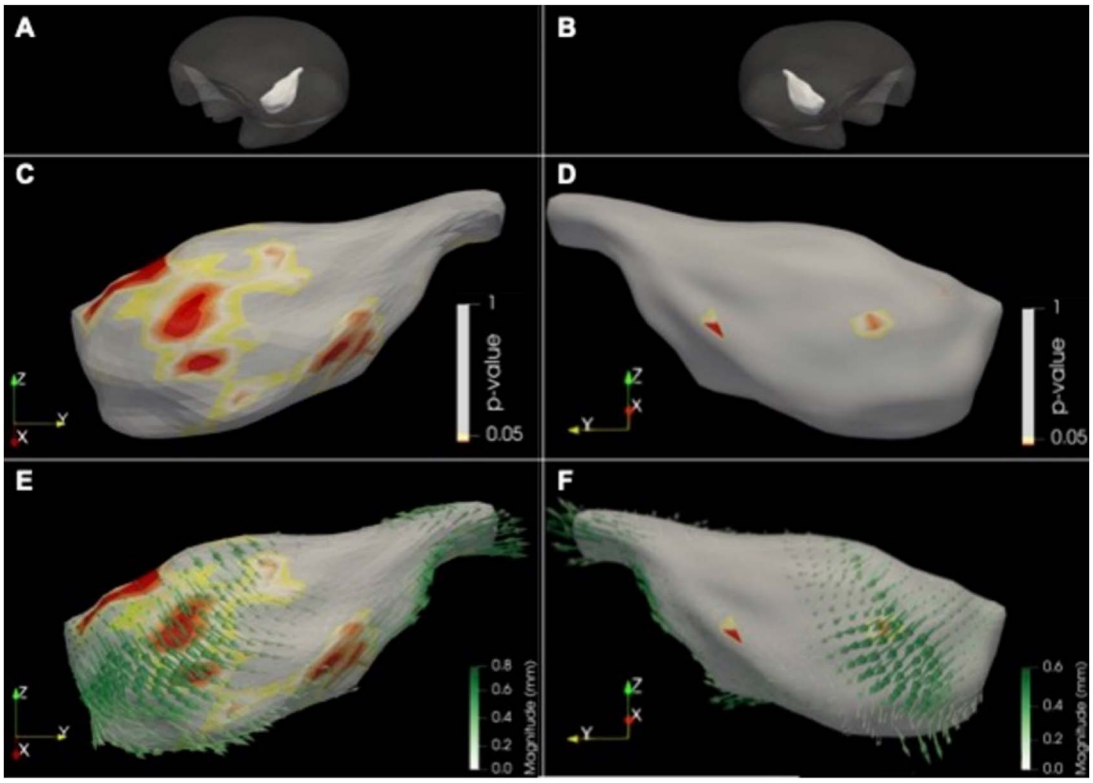

Fig. 2. Top row: Location of the left (A) and right (B) insula within the template brain. Middle row: False discovery rate-corrected *p*-value map highlighting regions of significant shape differences between dominant and subordinate monkeys in left (C) and right (D) insula. Bottom row: Same *p*-value map on the mean left (E) and right (F) subordinate monkeys' insula with overlayed vectors pointing in the direction of the mean dominant insula.

To determine whether structural differences were related to insula function, GCOR maps were generated. GCOR is a measure of the average correlation between activity in one brain region and activity in all other brain regions, reflecting the overall functional connectedness or centrality of the region of interest to the rest of the brain. GCOR was significantly lower in the left insula of monkeys who would eventually become dominant compared to those that would become subordinate. The lower insular GCOR in future dominant monkeys suggests that the left insula is less functionally coupled with other brain areas in these monkeys, potentially indicating more segregated or specialized processing. Consistent with this result, there was a trend towards lower fALFF in both the left and right insula of future dominant monkeys. fALFF quantifies the power of low frequency oscillations in the BOLD signal as a fraction of the total power across all measurable frequencies, reflecting the strength of regionally specific neural activity; fALFF is often observed to be altered in neuropsychiatric disorders. Although the difference did not reach statistical significance, the trend towards lower fALFF in monkeys that would eventually become dominant suggests reduced spontaneous insular activity that parallels the reduced connectivity seen in the GCOR analysis. These differences are not likely due to anesthesia. Although monkeys were anesthetized for the present studies, general anesthesia has been shown to reduce BOLD signal variability, enhancing the reliability of fALFF and connectivity measures and enabling optimal assessment of these measures during shorter scan times (Vedaei et al. 2022). Moreover, isoflurane has been shown to enhance regional contrast of fALFF via its hemodynamic effects (Wu et al. 2016). Finally, all scans occurred under identical conditions, further enhancing the confidence of our assessments.

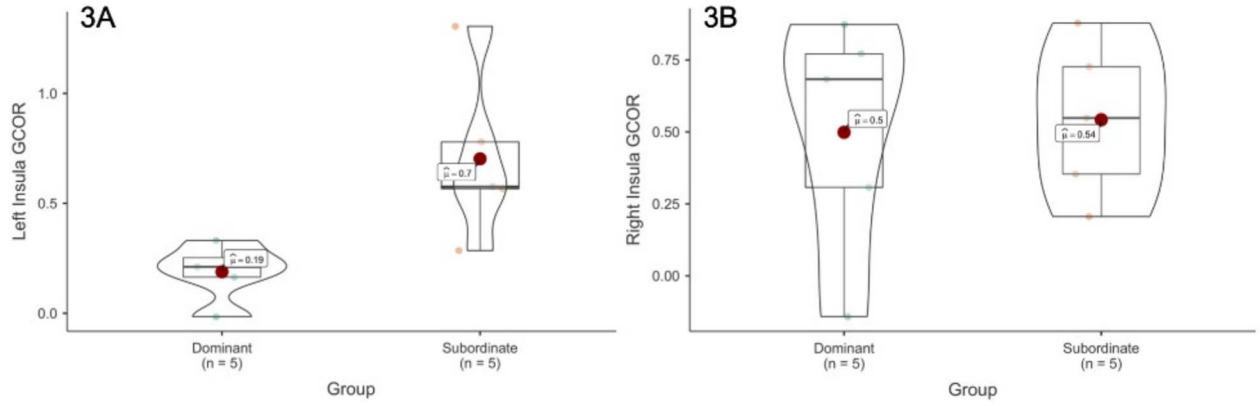

Fig. 3. Average global correlation (GCOR) from all voxels of left (1A) and right (1B) insula.

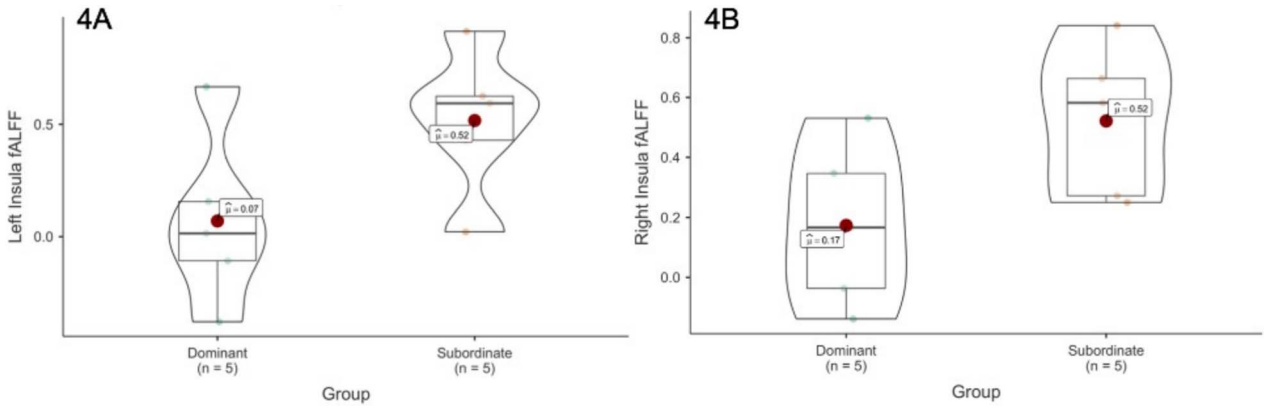

Fig. 4. fALFF from all voxels of left (1A) and right (1B) insula.

This study differed from others with a similar design in that our initial structural study was not brain-wide, but rather focused on the insula. We chose this approach because brain-wide analyses would have necessitated extensive corrections for multiple comparisons which, considering the relatively small sample size of the present study, would greatly reduce sensitivity. However, we subsequently performed exploratory analyses of other brain regions thought to be involved in establishment of the social hierarchy (bilateral amygdala, caudate nucleus, and prefrontal and frontal cortices) and negative control regions that are not thought to be involved (putamen, cerebellum and temporal auditory cortex). In none of these regions did volumes differ between monkeys that would become dominant and those that would become subordinate (Table 1). Consistent with this result, whole brain voxel-wise analyses of both GCOR and fALFF revealed no clusters of significant difference between the groups anywhere in the brain, most likely due to the small sample size and the very conservative correction implemented in voxel-wise analyses.

In summary, using complementary structural and functional MRI measures, we found evidence for altered left insular structure and functional dynamics that predicted future social rank in NHPs. Taken together, the lower GCOR and fALFF observed in monkeys that would become dominant might reflect a more selective, restricted pattern of insular function which could facilitate faster and more decisive responses to behaviorally relevant stimuli. Alternately, it might reflect a heightened awareness of subordinate monkeys to their surroundings. For example, socially subordinate monkeys face greater intimidation and overt aggression from dominant-ranked monkeys and thus may require more widespread brain activity to promote vigilance and processing of multiple social stimuli simultaneously. These findings are reminiscent of previous results demonstrating that patterns of brain activation during social confrontation differed in dominant and subordinate monkeys in brain areas associated with vigilance and emotional processing (Gould et al. 2017). The present findings suggest that individual differences in brain function in networks subserving social cognition exist prior to introduction to a social

Table 1. Comparisons of volumes for several brain regions between monkeys who would eventually become dominant versus subordinate.

Between-Group Volume Differences			
Region	**Test**	**Statistic**	**p**
R. Prefrontal Cortex	Student's t	−1.215925	0.25194
L. Prefrontal Cortex	Student's t	−1.195662	0.25941
R. Frontal Cortex	Student's t	1.275836	0.23085
L. Frontal Cortex	Student's t	1.124025	0.28726
R. Amygdala	Student's t	−0.98827	0.34633
L. Amygdala[a]	Welch's t	−0.809735	0.44155
R. Caudate[a]	Welch's t	0.580757	0.58008
L. Caudate[a]	Welch's t	1.038031	0.33617
R. Putamen	Student's t	1.360867	0.20343
L. Putamen	Student's t	0.960549	0.35943
R. Temporal Auditory Cortex	Student's t	0.258581	0.8012
L. Temporal Auditory Cortex	Student's t	0.06643	0.94834
R. Cerebellum	Student's t	0.83331	0.42413
L. Cerebellum	Student's t	0.901508	0.38852

Note. H_a μ Dom $\neq$ μ Sub [a]Levene's test is significant ($P < 0.05$); Welch's t-test was performed.

setting and could play a role in determining outcomes related to social dominance. Future research is required to characterize how the insula fits into networks with other brain structures implicated in dominance perception and social cognition, including the amygdala, prefrontal cortex and striatal regions.

Acknowledgments

The authors acknowledge the helpful contributions of Phillip Epperly, Miracle Collier and the staff of the WFUSM Translational Imaging Program. The sponsor played no role in the design, execution or presentation of these studies.

Author contributions

Paul W Czoty (Conceptualization, Funding acquisition, Project administration, Resources, Supervision), Mohammad Kawas (Data curation, Formal analysis, Methodology, Software, Validation, Visualization), Kedar Madi (Data curation, Formal analysis, Methodology, Software, Validation, Visualization), Richard Barcus (Data curation, Methodology, Validation, Visualization), Jeongchul Kim (Data curation, Methodology, Validation), Jeremy P Hudson (Data curation, Methodology, Validation), Lindsey K Galbo-Thomma (Investigation), Hongyu Yuan (Formal analysis, Methodology, Software, Validation), James B. Daunais (Conceptualization, Funding acquisition, Project administration), Christopher T. Whitlow (Conceptualization, Data curation, Formal analysis, Funding acquisition, Project administration, Supervision, Validation, Visualization).

Funding

Supported by National Institutes of Health/National Institute on Alcohol Abuse and Alcoholism grant numbers P50 AA026117 (P.W.C., project director; Jeffrey Weiner, P.I.) and T32 AA007565 (L.K.G.T. appointee to training grant).

Conflict of interest statement: The authors have no conflicts of interest to disclose.

References

Abbott DH et al. 2003. Are subordinates always stressed? A comparative analysis of rank differences in cortisol levels among primates. *Horm Behav*. 43:67–82. https://doi.org/10.1016/S0018-506X(02)00037-5.

Ahrens JP, Geveci B, Law CC. 2005. ParaView: An end-user tool for large-data visualization. In: Hansen CD, Johnson CR, editors. *The visualization*. New York (NY): Elsevier; pp. 717–131. 10.1016/B978-012387582-2/50038-1

Ashburner J. 2007. A fast diffeomorphic image registration algorithm. *NeuroImage*. 38:95–113. https://doi.org/10.1016/j.neuroimage.2007.07.007.

Ashburner J, Friston K. 1997. Multimodal image Coregistration and partitioning—a unified framework. *NeuroImage*. 6:209–217. https://doi.org/10.1006/nimg.1997.0290.

Ashburner J, Friston KJ. 2005. Unified segmentation. *NeuroImage*. 26:839–851. https://doi.org/10.1016/j.neuroimage.2005.02.018.

Behzadi Y, Restom K, Liau J, Liu TT. 2007. A component based noise correction method (CompCor) for BOLD and perfusion based fMRI. *NeuroImage*. 37:90–101. https://doi.org/10.1016/j.neuroimage.2007.04.042.

Bernstein IS. 1981. Dominance: the baby and the bathwater. *Behav Brain Sci*. 4:419–429. https://doi.org/10.1017/S0140525X00009614.

Brechbühler C, Gerig G, Kübler O. 1995. Parametrization of closed surfaces for 3-D shape description. *Comput Vis Image Underst*. 61:154–170. https://doi.org/10.1006/cviu.1995.1013.

Calhoun VD et al. 2017. The impact of T1 versus EPI spatial normalization templates for fMRI data analyses. *Hum Brain Mapp*. 38:5331–5342. https://doi.org/10.1002/hbm.23737.

Cauda F et al. 2012. Metaanalytic clustering of the insular cortex. *NeuroImage*. 62:343–355. https://doi.org/10.1016/j.neuroimage.2012.04.012.

Cerliani L et al. 2012. Probabilistic tractography recovers a rostrocaudal trajectory of connectivity variability in the human insular cortex. *Hum Brain Mapp*. 33:2005–2034. https://doi.org/10.1002/hbm.21338.

Chai XJ, Castañón AN, Ongür D, Whitfield-Gabrieli S. 2012. Anticorrelations in resting state networks without global signal regression. *NeuroImage*. 59:1420–1428. https://doi.org/10.1016/j.neuroimage.2011.08.048.

Chang LJ, Yarkoni T, Khaw MW, Sanfey AG. 2013. Decoding the role of the insula in human cognition: functional parcellation and large-scale reverse inference. *Cereb Cortex*. 23:739–749. https://doi.org/10.1093/cercor/bhs065.

Chiao JY, Mathur VA, Harada T, Lipke T. 2009. Neural basis of preference for human social hierarchy versus egalitarianism. *Ann N Y Acad Sci*. 1167:174–181. https://doi.org/10.1111/j.1749-6632.2009.04508.x.

Cloutman LL, Binney RJ, Drakesmith M, Parker GJM, Lambon Ralph MA. 2012. The variation of function across the human insula mirrors its patterns of structural connectivity: evidence from in vivo probabilistic tractography. *NeuroImage*. 59:3514–3521. https://doi.org/10.1016/j.neuroimage.2011.11.016.

Czoty PW, Nader MA. 2012. Individual differences in the effects of environmental stimuli on cocaine choice in socially housed male cynomolgus monkeys. *Psychopharmacology*. 224:69–79. https://doi.org/10.1007/s00213-011-2562-3.

Czoty PW, Gould RW, Nader MA. 2009. Relationship between social rank and cortisol and testosterone concentrations in male cynomolgus monkeys (Macaca fascicularis). *J Neuroendocrinol*. 21:68–76. https://doi.org/10.1111/j.1365-2826.2008.01800.x.

Downar J, Crawley AP, Mikulis DJ, Davis K. 2000. A multimodal cortical network for the detection of changes in the sensory environment. *Nat Neurosci*. 3:277–283. https://doi.org/10.1038/72991.

Eimer M. 2011. The face-sensitivity of the N170 component. *Front Hum Neurosci*. 5:119. https://doi.org/10.3389/fnhum.2011.00119.

Evrard HC. 2019. The organization of the primate insular cortex. *Front Neuroanat*. 13:43. https://doi.org/10.3389/fnana.2019.00043.

Evrard HC, Logothetis NK, Bud Craig AD. 2014. Modular architectonic organization of the insula in the macaque monkey: architectonic organization of macaque insula. *J Comp Neurol*. 522:64–97. https://doi.org/10.1002/cne.23436.

Farrow TFD et al. 2011. Higher or lower? The functional anatomy of perceived allocentric social hierarchies. *NeuroImage*. 57:1552–1560. https://doi.org/10.1016/j.neuroimage.2011.05.069.

Friston KJ et al. 1995. Spatial registration and normalization of images. *Hum Brain Mapp*. 3:165–189. https://doi.org/10.1002/hbm.460030303.

Friston KJ, Williams S, Howard R, Frackowiak RS, Turner R. 1996. Movement-related effects in fMRI time-series. *Magn Reson Med*. 35:346–355. https://doi.org/10.1002/mrm.1910350312.

Galbo LK et al. 2022. Social dominance in monkeys: lack of effect on ethanol self-administration during schedule induction. *Alcohol*. 98:1–7. https://doi.org/10.1016/j.alcohol.2021.10.001.

Galbo-Thomma LK, Davenport AT, Epperly PM, Czoty PW. 2023. Influence of social rank on the development of long-term ethanol drinking trajectories in cynomolgus monkeys. *Alcohol Clin Exp Res*. 47(10):1943–1951. https://doi.org/10.1111/acer.15163.

Gesquiere LR et al. 2011. Life at the top: rank and stress in wild baboons. *Science*. 333:357–360. https://doi.org/10.1126/science.1207120.

Gould RW, Czoty PW, Porrino LJ, Nader MA. 2017. Social status in monkeys: effects of social confrontation on brain function and cocaine self-administration. *Neuropsychopharmacology*. 42: 1093–1102. https://doi.org/10.1038/npp.2016.285.

Hallquist MN, Hwang K, Luna B. 2013. The nuisance of nuisance regression: spectral misspecification in a common approach to resting-state fMRI preprocessing reintroduces noise and obscures functional connectivity. *NeuroImage*. 82:208–225. https://doi.org/10.1016/j.neuroimage.2013.05.116.

Hsu M, Anen C, Quartz S. 2008. The right and the good: distributive justice and neural encoding of equity and efficiency. *Science*. 320: 1092–1095. https://doi.org/10.1126/science.1153651.

Hu J et al. 2016. Social status modulates the neural response to unfairness. *Soc Cogn Affect Neurosci*. 11:1–10. https://doi.org/10.1093/scan/nsv086.

Jenkinson M, Smith S. 2001. A global optimisation method for robust affine registration of brain images. *Med Image Anal*. 5:143–156. https://doi.org/10.1016/S1361-8415(01)00036-6.

Jenkinson M, Bannister P, Brady M, Smith S. 2002. Improved optimization for the robust and accurate linear registration and motion correction of brain images. *NeuroImage*. 17:825–841. https://doi.org/10.1006/nimg.2002.1132.

Jenkinson M, Beckmann CF, Behrens TE, Woolrich MW, Smith SM. 2012. FSL. *NeuroImage*. 62:782–790. https://doi.org/10.1016/j.neuroimage.2011.09.015.

Jezzini A, Caruana F, Stoianov I, Gallese V, Rizzolatti G. 2012. Functional organization of the insula and inner perisylvian regions. *Proc Natl Acad Sci*. 109:10077–10082. https://doi.org/10.1073/pnas.1200143109.

Johnson SL, Leedon LJ, Muhtadie L. 2012. The dominance behavioral system and psychopathology: evidence from self-report, observational, and biological studies. *Psychol Bull*. 138:692–743. https://doi.org/10.1037/a0027503.

Kaplan JR, Chen H, Manuck SB. 2009. The relationship between social status and atherosclerosis in male and female monkeys as revealed by meta-analysis. *Am J Primatol*. 2:359–368.

Katabathula S, Wang Q, Xu R. 2021. Predict Alzheimer's disease using hippocampus MRI data: a lightweight 3D deep convolutional network model with visual and global shape representations. *Alzheimers Res Ther*. 13:104.

Kim SH et al. 2023. Anterior insula-associated social novelty recognition: pivotal roles of a local retinoic acid cascade and oxytocin signaling. *Am J Psychiatry*. 180:305–317. https://doi.org/10.1176/appi.ajp.21010053.

Knobloch S et al. 2024. Empathy in schizophrenia: neural alterations during emotion recognition and affective sharing. *Front Psychiatry*. 15:1288028. https://doi.org/10.3389/fpsyt.2024.1288028.

Kumaran D, Melo HL, Duzel E. 2012. The emergence and representation of knowledge about social and nonsocial hierarchies. *Neuron*. 76:653–666. https://doi.org/10.1016/j.neuron.2012.09.035.

Kurth F, Zilles K, Fox PT, Laird AR, Eickhoff SB. 2010. A link between the systems: functional differentiation and integration within the human insula revealed by meta-analysis. *Brain Struct Funct*. 214: 519–534. https://doi.org/10.1007/s00429-010-0255-z.

Li S, Kreuger F, Camilleri JA, Eickhoff AB, Qu C. 2021. The neural signature of social hierarchy-related learning and interaction: a coordinate- and connectivity-based meta-analysis. *NeuroImage*. 245:118731. https://doi.org/10.1016/j.neuroimage.2021.118731.

Ligneul R, Obeso I, Ruff CC, Dreher JC. 2016. Dynamical representation of dominance relationships in the human rostromedial prefrontal cortex. *Curr Biol*. 26:3107–3115. https://doi.org/10.1016/j.cub.2016.09.015.

Ligneul R, Girard R, Dreher JC. 2017. Social brains and divides: the interplay between social dominance orientation and the neural sensitivity to hierarchical ranks. *Sci Rep*. 7:45920. https://doi.org/10.1038/srep45920.

Ly M, Haynes MR, Barter JW, Weinberger DR, Zink CF. 2011. Subjective socioeconomic status predicts human ventral striatal responses to social status information. *Curr Biol*. 21:794–797. https://doi.org/10.1016/j.cub.2011.03.050.

Madi K. 2021. Development of an automated pipeline to analyze hippocampal morphometry in response to neurodegenerative diseases. *Department of Biomedical Engineering*. Winston-Salem: Wake Forest University; p. 121.

Marsh AA, Blair KS, Jones MM, Soliman N, Blair RJR. 2009. Dominance and submission: the ventrolateral prefrontal cortex and responses to cues. *J Cognitive Neurosci*. 21:713–724. https://doi.org/10.1162/jocn.2009.21052.

Michoud L et al. 2019. A web-based system for statistical shape analysis in temporomandibular joint osteoarthritis. *Proc SPIE Int Soc Opt Eng*. (Feb):10953:109305T.

Munuera J, Rigotti M, Salzman CD. 2018. (2018): shared neural coding for social hierarchy and reward value in primate amygdala. *Nat Neurosci*. 21:415–423. https://doi.org/10.1038/s41593-018-0082-8.

Nader MA, Czoty PW, Nader SH, Morgan D. 2012a. Nonhuman primate models of social behavior and cocaine abuse. *Psychopharmacology*. 224:57–67. https://doi.org/10.1007/s00213-012-2843-5.

Nader MA et al. 2012b. Social dominance in female monkeys: dopamine receptor function and cocaine reinforcement. *Biol Psychiatry*. 72:414–421. https://doi.org/10.1016/j.biopsych.2012.03.002.

Naqvi NH, Rudrauf D, Damasio H, Bechara A. 2007. Damage to the insula disrupts addiction to cigarette smoking. *Science*. 315: 531–534. https://doi.org/10.1126/science.1135926.

Nieto-Castanon A. 2022. Preparing fMRI data for statistical analysis. arXiv:2210.13564v1. https://doi.org/10.48550/arXiv.2210.13564

Nieto-Castanon A. 2020a. FMRI denoising pipeline. In: Nieto-Castanon A, editors. *Handbook of functional connectivity magnetic resonance imaging methods in CONN*. Boston (MA): Hilbert Press; pp. 17–25. 10.56441/hilbertpress.2207.6600

Nieto-Castanon A. 2020b. FMRI minimal preprocessing pipeline. In: Nieto-Castanon A, editors. *Handbook of functional connectivity magnetic resonance imaging methods in CONN*. Boston (MA): Hilbert Press; pp. 3–16 10.56441/hilbertpress.2207.6599

Noonan MP et al. 2014. A neural circuit covarying with social hierarchy in macaques. *PLoS Biol*. 12:e1001940. https://doi.org/10.1371/journal.pbio.1001940.

Paniagua B et al. 2013. Lateral ventricle morphology analysis via mean latitude axis. Proc SPIE Int Soc. *Opt Eng*. 8672:2006846.

Power JD et al. 2014. Methods to detect, characterize, and remove motion artifact in resting state fMRI. *NeuroImage*. 84:320–341. https://doi.org/10.1016/j.neuroimage.2013.08.048.

Saad ZS et al. 2013. Correcting brain-wide correlation differences in resting-state FMRI. *Brain Connect*. 3:339–352. https://doi.org/10.1089/brain.2013.0156.

Sallet J et al. 2011. Social network size affects neural circuits in macaques. *Science*. 334:697–700. https://doi.org/10.1126/science.1210027.

Santamaria-Garcia H, Burgaleta M, Sebastian-Gales N. 2015. Neuroanatomical markers of social hierarchy recognition in humans: a combined ERP/MRI study. *J Neurosci*. 35:10843–10850. https://doi.org/10.1523/JNEUROSCI.1457-14.2015.

Sapolsky RM. 2005. The influence of the primate social hierarchy on primate health. *Science*. 308:648–652. https://doi.org/10.1126/science.1106477.

Seeley WW. 2019. The salience network: a neural system for perceiving and responding to homeostatic demands. *J Neurosci*. 39:9878–9882. https://doi.org/10.1523/JNEUROSCI.1138-17.2019.

Studholme C, Hawkes DJ, Hill DL. 1998. Normalized entropy measure for multimodality image alignment. *Proc SPIE*. 3338. https://doi.org/10.1117/12.310835.

Styner M et al. 2006. Framework for the statistical shape analysis of brain structures using SPHARM-PDM. *Insight J*. 1071:242–250. https://doi.org/10.54294/owxzil.

Styner M et al. 2007. Automatic brain segmentation in rhesus monkeys. *Proc SPIE*. 65122:65122L.

Sypre L, Durand J-B, Nelissen K. 2023. Functional characterization of macaque insula using task-based and resting-state fMRI. *NeuroImage*. 276:120217. https://doi.org/10.1016/j.neuroimage.2023.120217.

Tustison NJ et al. 2010. N4ITK: improved N3 bias correction. *IEEE Trans Med Imaging*. 29:1310–1320. https://doi.org/10.1109/TMI.2010.2046908.

Uddin LQ, Nomi JS, Hébert-Seropian B, Ghaziri J, Boucher O. 2017. Structure and function of the human insula. *J Clin Neurophysiol*. 34:300–306. https://doi.org/10.1097/WNP.0000000000000377.

Vedaei F, Alizadeh M, Romo V, Mohamed FB, Wu C. 2022. The effect of general anesthesia on the test-retest reliability of resting-state fMRI metrics and optimization of scan length. *Front Neurosci*. 16:937172. https://doi.org/10.3389/fnins.2022.937172.

Vicory J et al. 2018. SlicerSALT: shape AnaLysis toolbox. *Shape Med Imaging*. 11167:65–72. https://doi.org/10.1007/978-3-030-04747-4_6 Cham, Springer International Publishing.

Voineskos AN et al. 2015. Hippocampal (subfield) volume and shape in relation to cognitive performance across the adult lifespan. *Hum Brain Mapp*. 36:3020–3037. https://doi.org/10.1002/hbm.22825.

Wang X et al. 2021. U-net model for brain extraction: trained on humans for transfer to non-human primates. *NeuroImage*. 235:118001. https://doi.org/10.1016/j.neuroimage.2021.118001.

Watanabe N and Yamamoto M. 2015. Neural mechanisms of social dominance. *Front Neurosci*. 9:154.

Whitfield-Gabrieli S, Nieto-Castanon A, Ghosh S. 2011. Artifact detection tools (ART) Cambridge (MA): Release Version. 7:11.

Whitfield-Gabrieli S, Nieto-Castanon A. 2012. CONN: a functional connectivity toolbox for correlated and anticorrelated brain networks. *Brain Connect*. 2:125–141. https://doi.org/10.1089/brain.2012.0073.

Wu TL et al. 2016. Effects of isoflurane anesthesia on resting-state fMRI signals and functional connectivity within primary somatosensory cortex of monkeys. *Brain Behavior*. 6:e00591. https://doi.org/10.1002/brb3.591.

Zaki J, Davis JI, Ochsner KN. 2012. Overlapping activity in anterior insula during interoception and emotional experience. *NeuroImage*. 62:493–499. https://doi.org/10.1016/j.neuroimage.2012.05.012.

Zink CF et al. 2008. Know your place: neural processing of social hierarchy in humans. *Neuron*. 58:273–283. https://doi.org/10.1016/j.neuron.2008.01.025.

Zou QH et al. 2008. An improved approach to detection of amplitude of low-frequency fluctuation (ALFF) for resting-state fMRI: fractional ALFF. *J Neurosci Methods*. 172:137–141. https://doi.org/10.1016/j.jneumeth.2008.04.012.

Cerebral Cortex, 2025, **35**, bhaf043
https://doi.org/10.1093/cercor/bhaf043
Original Article